SCIENCE CHINA
Earth Sciences

• RESEARCH PAPER •

November 2015 Vol.58 No.11: 2049–2058
doi: 10.1007/s11430-015-5093-7

Turbulence and mixing in a freshwater-influenced tidal bay: Observations and numerical modeling

LIAN Qiang[1,2] & LIU ZhiYu[1,2*]

[1] *Department of Physical Oceanography, College of Ocean & Earth Sciences, Xiamen University, Xiamen 361102, China;*
[2] *State Key Laboratory of Marine Environmental Science, Xiamen University, Xiamen 361102, China*

Received December 26, 2014; accepted March 6, 2015; published online May 15, 2015

In situ observations and numerical simulations of turbulence are essential to understanding vertical mixing processes and their dynamical controls on both physical and biogeochemical processes in coastal embayments. Using *in situ* data collected by bottom-mounted acoustic Doppler current profilers (ADCPs) and a free-falling microstructure profiler, as well as numerical simulations with a second-moment turbulence closure model, we studied turbulence and mixing in the Xiamen Bay, a freshwater-influenced tidal bay located at the west coast of the Taiwan Strait. Dynamically, the bay is driven predominantly by the M_2 tide, and it is under a significant influence of the freshwater discharged from the Jiulong River. It is found that turbulence quantities such as the production and dissipation rates of the turbulent kinetic energy (TKE) were all subject to significant tidal variations, with a pronounced ebb-flood asymmetry. Turbulence was stronger during flood than ebb. During the flooding period, the whole water column was nearly well mixed with the depth-averaged TKE production rate and vertical eddy viscosity being up to 5×10^{-6} W kg^{-1} and 2×10^{-2} m^2 s^{-1}, respectively. In contrast, during the ebb strong turbulence was confined only to a 5–8 m thick bottom boundary layer, where turbulence intensity generally decreases with distance from the seafloor. Diagnosis of the potential energy anomaly showed that the ebb-flood asymmetry in turbulent dissipation and mixing was due mainly to tidal straining process as a result of the interaction between vertically shared tidal currents and horizontal density gradients. The role of vertical mixing in generating the asymmetry was secondary. A direct comparison of the modeled and observed turbulence quantities confirmed the applicability of the second-moment turbulence closure scheme in modeling turbulent processes in this weakly stratified tidally energetic environment, but also pointed out the necessity of further refinements of the model.

tidal bay, turbulent mixing, second-moment turbulence closure model, turbulent kinetic energy dissipation rate, vertical eddy viscosity

Citation: Lian Q, Liu Z Y. 2015. Turbulence and mixing in a freshwater-influenced tidal bay: Observations and numerical modeling. Science China: Earth Sciences, 58: 2049−2058, doi: 10.1007/s11430-015-5093-7

Turbulent mixing is the key process controlling vertical exchanges in coastal embayments. The turbulent fluxes of heat, materials, and momentum driven by turbulence play a vital role in setting vertical structures of water column and can affect a variety of physical as well as biogeochemical processes.

In recent years, the development of broad-band acoustic Doppler current profilers (ADCPs) and commercial microstructure profilers greatly strengthens our capability to measure turbulence quantities, such as the production and dissipation rates of the turbulent kinetic energy (TKE), in shelf seas and coastal embayments (Rippeth et al., 2003; Liu et al., 2009; Simpson et al., 2009; Lucas et al., 2014), and in consequence significantly advanced our understanding of turbulent mixing processes in these systems. As a

*Corresponding author (email: zyliu@xmu.edu.cn)

result, it has become possible to understand both characteristics and generation mechanisms of turbulence, as well as its dynamic controls on a variety of physical and biogeochemical processes, and to assess the capability of the state-of-the-art turbulence closure schemes in modeling TKE budgets and mixing.

High-frequency broad-band ADCPs measure along-beam velocities based on the Doppler effect. With these measurements, turbulence quantities such as the Reynolds stress and vertical eddy viscosity can be estimated with the Variance Method, which was first applied on the continental shelf (Lohrmann et al., 1990) and then extended to coastal embayments (Lu and Lueck, 1999a, 1999b; Stacey et al., 1999a, 1999b; Rippeth et al., 2003).

The free-falling microstructure profilers measure microscale velocity shear with air-foil shear probes (Dewey et al., 1987; Prandke and Stips, 1998). By adopting the isotropy assumption for small-scale turbulence, the dissipation rate of TKE, commonly termed as ε, is estimated from these data. Lueck et al. (2002) provided a systematic review on the shear-probe construction and details of data processing, as well as the historical aspects of this technique and its applications. This technique has been widely used in shelf sea (Simpson et al., 1996; Liu et al., 2009) and estuary studies (Fisher et al., 2002).

In ocean modeling, turbulent mixing is conventionally described by either constant mixing coefficients (Kraus and Turner, 1967) or semi-empirical formulations (Simpson et al., 1991). Such models, however, cannot take into account many of the occurring complex physical phenomena. Nowadays, turbulent mixing is usually modeled with second-moment turbulence closure schemes (Burchard and Bolding, 2001; Umlauf and Burchard, 2005), which are derived from the second-moment transport equations with certain approximations. As compared to the bulk or integrated models, the second-moment turbulence closure schemes retain more information of turbulence, and are therefore physically sounder, numerically more robust, and with a much higher predictive ability. However, direct turbulence measurements-based assessment of the turbulence closure schemes has been lacking (Simpson et al., 1996).

In this paper, we provide a detailed analysis of characteristics of turbulence and mixing, as well as their temporal and spatial variabilities, in a freshwater-influenced tidal bay, the Xiamen Bay, on the basis of *in situ* turbulence measurements. These results, along with simultaneous observations of current and stratification, allow us to have a direct assessment of the start-of-the-art turbulence closure schemes in modeling turbulence characteristics and variabilities in this complex dynamic regime. We conclude that the turbulence closure schemes work pretty well in weakly stratified tidally energetic environment, although the necessity of further refinements is quite obvious. The tidal asymmetry as well as other distinct features of turbulent mixing could be correctly modeled.

1 Study area and the experiment

The Xiamen Bay (XB) is a typical semi-enclosed bay at the west side of the Taiwan Strait (Figure 1). The water depth in the bay ranges from 5 to 20 m. The bay occupies an area of about 900 km^2 and consists of numerous islands of various size, such as the Xiamen, Gulangyu, and Kinmen Islands. Tides in the XB are predominantly semi-diurnal, and tidal currents are rectilinear. The maximum tidal range and current speed are up to 6.0 m and 1.5 m s^{-1}, respectively. As a result of the strong (vertically sheared) tidal currents and pronounced horizontal density gradients due to the freshwater discharged from the Jiulong Rive, tidal straining process is expected to occur in the XB.

A cruise for the observation of turbulence and mixing in the XB was carried out in March 2011. The measurements consist of 50-h continuous measurements at three sites (A1, A2, and M3, Figure 1) from March 17 to March 19. These sites were located within a relatively small region (24°25.91′N–24°26.14′N, 118°03.63′E–118°03.76′E) with the mean water depth of about 20 m. At St. M3, turbulence

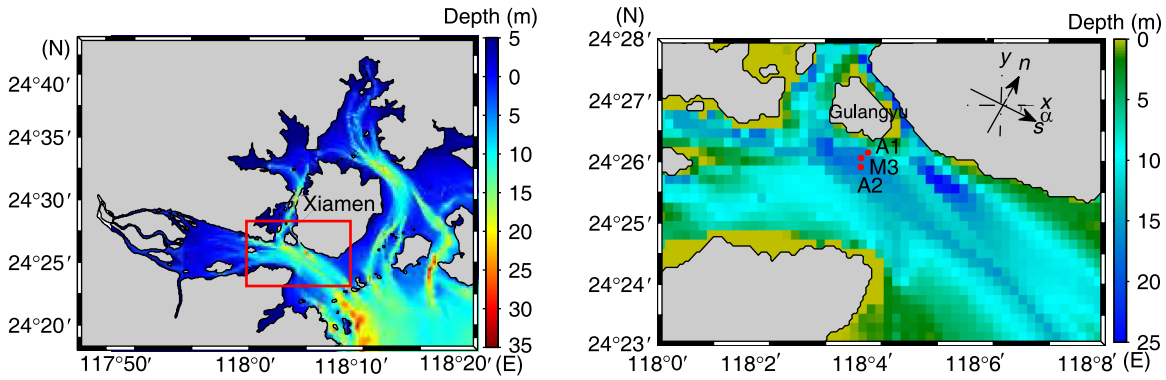

Figure 1 Bathymetry around the Xiamen Island shown in meters above the theoretical lowest tide level. A1 and A2 are two mooring stations; M3 is the station where microstructure profiling measurements were conducted.

profiling measurements were conducted with an MSS-60 microstructure profiler (Liu et al., 2009), whereas velocity vector through the whole water column was measured by a 600 kHz ship-mounted ADCP. Mooring measurements were conducted at the other two sites, with along-beam velocity data being collected by two bottom-mounted ADCPs. The St. A1 was located 200 m off-shore from the Gulangyu Island with a water depth of about 19.4 m. The current at this site was measured with a bottom-mounted 300 kHz ADCP, with samples being recorded every 2 s from 17 to 19 May. The bin size is 1.0 m. The St. A2 was in the center of the channel (21.6 m depth), about 480 m from St. A1. The current profiles at this site were measured with a bottom-mounted 600 kHz ADCP, which recorded samples every 2 s with a vertical bin size of 0.5 m. The St. M3 was located at the middle of Sts. A1 and A2, with a water depth of about 20.1 m. Every 30 min, a group of three consecutive casts of the MSS profiler was launched within 2–3 min to obtain estimates of the TKE dissipation rate.

The weather was very quiet during the observational period: wind speed at 10 m above the sea surface was mostly below 2.0 m s^{-1}. The wind stress was therefore negligible compared to the frictional stress at the bottom due to strong tidal currents. Figure 2(a) shows the 10-min averaged velocity at 4.73 m above the seafloor. It can be seen that the flow in the bay was almost rectilinear, in the direction of northwest to southeast, roughly parallel to the coastal line of the Gulangyu Island. Figure 2(b) shows the results of tidal harmonic analysis, which extracts main tidal constituents from the current measurements. Six major constituents, including M_2, O_1, K_1, S_2, M_4 and MS_4, were included in the analysis. As shown in Figure 2(b), the along-channel velocity component, u_s, was up to 0.8 m s^{-1}, much larger than the cross-channel component, u_n.

2 Data analysis and numerical simulation

2.1 Turbulence measurements with ADCP

In the past decade, high-frequency broad-band ADCP has become a useful tool for measuring turbulence in shallow waters. It is based on the Variance Method as mentioned before. By assuming that second moments of turbulent fluctuations are homogeneous within the spreading area of the four beams of ADCP, the Reynolds stress can be calculated from the variances of the four along-beam velocity components. The TKE production rate and vertical eddy viscosity are then calculated from the Reynolds stress and the vertical shear of the mean horizontal current. Here we briefly introduce the detailed formulations below.

According to the Reynolds decomposition principle, the along-beam velocity b_i (i=1,…,4) can be decomposed into a statistic mean and a turbulent fluctuation, that is, $b_i=\langle b_i\rangle + b_i'$. Here, $\langle b_i\rangle$ is the mean (defined as 10-min average in this study), and b_i' the fluctuation. Let beams 1 and 2 be in the x-z plane, and beams 3 and 4 in the y-z plane, the two horizontal components of the Reynolds stress can be estimated from the variance of b_i' (e.g., Stacey et al., 1999b),

$$\frac{\tau_x}{\rho} = -\langle u'w'\rangle = \frac{\langle b_2'^2\rangle - \langle b_1'^2\rangle}{2\sin 2\theta}, \quad (1)$$

$$\frac{\tau_y}{\rho} = -\langle v'w'\rangle = \frac{\langle b_4'^2\rangle - \langle b_3'^2\rangle}{2\sin 2\theta}, \quad (2)$$

where (u', v', w') are velocity fluctuations in the Cartesian coordinates, $\langle b_i'^2\rangle$ is variance of the along-beam velocity b_i, and θ is the angle of each beam relative to the axis of the instrument (θ=20° for the ADCPs used in this study).

The rate at which kinetic energy is transferred from the

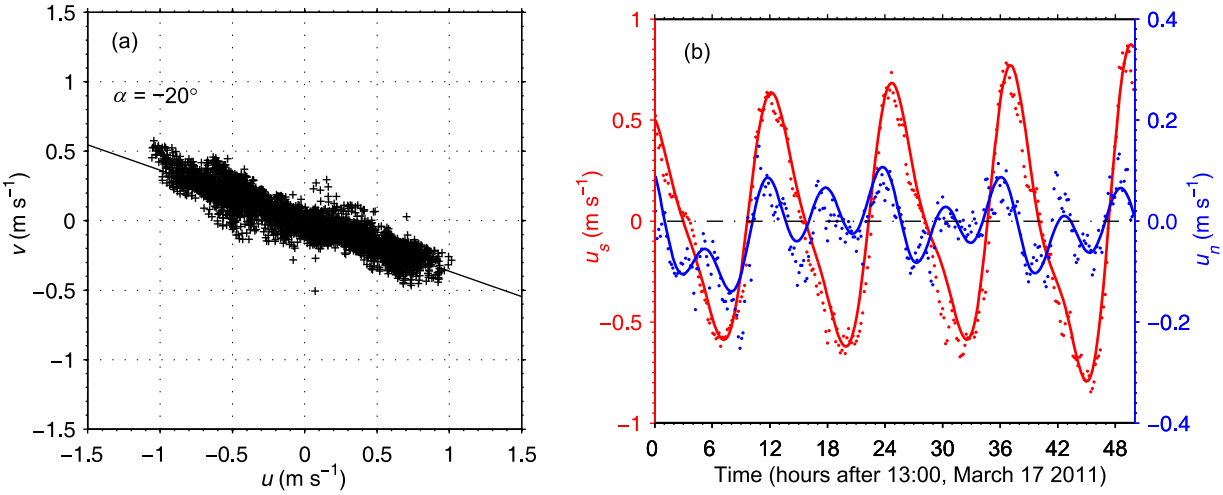

Figure 2 (a) The 10-min averaged velocity at St. A1, α is the angle of major axis from true north, it was determined by a best fit to the directions of the 10-min averaged velocity vector at all the heights above 4.73 m ; (b) the observed (red and blue dots) and tidal (red and blue lines) currents (u_s, u_n) at 4.73 m above the seafloor.

mean flow to turbulence through the interaction of turbulence with the shear of the mean flow is defined as the shear production of TKE, termed as P here, that is

$$P = -\langle u'w' \rangle \frac{\partial \langle u \rangle}{\partial z} - \langle v'w' \rangle \frac{\partial \langle v \rangle}{\partial z}, \tag{3}$$

where $\langle u'w' \rangle$ and $\langle v'w' \rangle$ can be estimated from eqs. (1) and (2), and $\partial\langle u \rangle/\partial z$ and $\partial\langle v \rangle/\partial z$ are the horizontal components of the mean flow shear.

Another important turbulence quantity that describes the effects of turbulent motions on the mean flow is the vertical eddy viscosity, υ_t. According to the eddy viscosity hypothesis (e.g., Schmitt, 2007), the eddy viscosity can be estimated as

$$\upsilon_t = P / S^2 = P \Bigg/ \left(\left(\frac{\partial \langle u \rangle}{\partial z} \right)^2 + \left(\frac{\partial \langle v \rangle}{\partial z} \right)^2 \right), \tag{4}$$

where S^2 (unit: s^{-2}) is the square of mean shear.

2.2 Microstructure profiling measurements

The free-falling microstructure profiler such as the Microstructure Sampling System (MSS) or the Fast Light Yo-yo (FLY) measures micro-scale velocity shear with two shear probes mounted in the front of the instrument (Prandke and Stips, 1998). By adopting the isotropy assumption for small-scale turbulence, the TKE dissipation rate ε can be estimated as

$$\varepsilon = \frac{15}{2} \upsilon \int_0^\infty E_{\partial u'/\partial z}(k) \mathrm{d}k = \frac{15}{2} \upsilon \left\langle \left(\frac{\partial u}{\partial z} \right)^2 \right\rangle, \tag{5}$$

where υ is the kinematic molecular viscosity of seawater ($\upsilon \approx 1.3\times10^{-6}$ m^2 s^{-1}), $k=2\pi/\lambda$ is the vertical wavenumber (λ is the vertical wavelength), $E_{\partial u'/\partial z}(k)$ is the wavenumber spectrum of velocity shear $\partial u'/\partial z$, and $\langle \cdots \rangle$ indicates a spatial or ensemble average.

When the temporal variation and transports of TKE are negligible, the shear production is locally balanced by viscous dissipation and buoyancy flux, that is $P=B+\varepsilon$. If the stratification is weak ($B\approx0$), the balance is further simplified to $P=\varepsilon$, suggesting a local balance of production and dissipation of TKE. More generally, for a stably stratified shear flow ($B>0$), the combination of the mean shear squared S^2, stratification $N^2=(-g/\rho_0)\partial\rho/\partial z$ and an estimated/assumed flux Richardson number R_f can be used to estimate the vertical eddy viscosity υ_t and eddy diffusivity υ_t' as follows (e.g., Stacey et al., 1999a)

$$\upsilon_t = \frac{1}{1-R_f} \frac{\varepsilon}{S^2}, \tag{6}$$

$$\upsilon_t' = \frac{R_f}{1-R_f} \frac{\varepsilon}{N^2} = \Gamma \frac{\varepsilon}{N^2}, \tag{7}$$

where $R_f = B/P$, and $\Gamma = R_f/(1-R_f)$ is the mixing efficiency. In general, Γ is not a constant, but is closely related to the generation and evolution of turbulence. However, current knowledge on physical mechanisms controlling the mixing efficiency is very limited. For naturally occurring stratified shear flows, the mixing efficiency is usually assumed to be around 0.2 for estimating υ_t and υ_t' (Thorpe, 2007).

2.3 Second-moment turbulence closure models

The second-moment turbulence closure model (hereafter referred to as the SMC model) simulates certain second moments of turbulence fluctuations by solving their transport equations (Umlauf and Burchard, 2005). For example, with the conventions $u_1=u$, $u_2=v$, and $u_3=w$, the transport equations for the Reynolds stress can be written in the following form

$$D_t \langle u_i' u_j' \rangle - \psi_{ij} = P_{ij} + \Omega_{ij} + B_{ij} + \Pi_{ij} - \varepsilon_{ij} \quad (i,j=1,2,3), \tag{8}$$

where D_t represents the material derivative, P_{ij} and B_{ij} the production of Reynolds stress by mean shear and buoyancy, respectively. ψ_{ij} and Π_{ij} are terms responsible for distributing momentum in physical space and between the components of the Reynolds stress tensor, Ω_{ij} a term reflecting the effect of rotation, and ε_{ij} the viscous dissipation rate of the Reynolds stress tensor. A precise definition of all terms can be found in a review paper by Umlauf and Burchard (2005).

A transport equation for TKE can be derived directly from (8) by setting $i=j$:

$$\partial_t k - \partial_z \left(\frac{\upsilon_t}{\sigma_k} \partial_z k \right) = P + B - \varepsilon, \tag{9}$$

where $k = 1/2 \langle u_i'^2 \rangle$ is the TKE per unit mass, the abbreviations $P = 1/2 P_{ij}$ and $B = 1/2 B_{ij}$ are the shear production and buoyancy production of TKE, and $\varepsilon = 1/2 \varepsilon_{ij}$ is the TKE dissipation rate.

Similarly, an exact transport equation for the TKE dissipation rate ε can also be derived from the Navier-Stokes equations (Wilocx, 1998), but it is not a practically useful starting point for a model equation given its very high complexity. The most common approach is to model the right-hand side of the ε equation as scaled linear combinations of the three terms on the right-hand side of the k equation. This modeling strategy leads to the following closed form of the ε equation:

$$\partial_t \varepsilon - \partial_z \left(\frac{\upsilon_t}{\sigma_\varepsilon} \partial_z \varepsilon \right) = \frac{\varepsilon}{k} \left(C_{\varepsilon 1} P + C_{\varepsilon 3} B - C_{\varepsilon 2} \varepsilon \right). \tag{10}$$

The eqs. (9) and (10) form the so-called k-ε model, which is widely used in turbulence simulations (Burchard

and Bolding, 2001; Pope, 2000). Commonly-used values of the parameters read ($C_{\varepsilon 1}$, $C_{\varepsilon 2}$, $C_{\varepsilon 3}$, σ_k, σ_ε)=(1.44, 1.92, 1.0, 1.0, 1.08). The vertical eddy viscosity υ_t resulting from this closure is of the following form

$$\upsilon_t = C_\mu \frac{k^2}{\varepsilon}, \tag{11}$$

where C_μ is the non-dimensional stability function that represents the effects of stratification and velocity shear. All the information of the second moments is now included in C_μ. Different parameterisations of the stability function form different turbulence closure schemes (Burchard and Bolding, 2001). Here, we use a set of stability functions proposed by Canuto et al. (2001).

3 Results

3.1 The Reynolds stress

The Reynolds stress is a basic turbulence quantity that is commonly estimated in both observations and numerical simulations. To reveal the tidal variability of the Reynolds stress, the Reynolds stress components (τ_x, τ_y) calculated from eqs. (2) and (3) were first projected onto the along- and cross-channel directions, that is (τ_s, τ_n). It is evident that the stress was roughly in the along-channel direction, i.e., τ_n was much less than τ_s as one would expect.

Figure 3 shows the along-channel Reynolds stress component τ_s and the corresponding vertical shear of the mean flow, $\partial u_s/\partial z$, at the Sts. A1 and A2. It can be found that both τ_s and $\partial u_s/\partial z$ were subject to significant semi-diurnal variations, with an evident ebb-flood asymmetry. They were larger during the flood than during the ebb. On food tide, the along-channel stress is negative (~−10 cm^2 s^{-2}), suggesting an upward transport of horizontal momentum due to the interaction of tidal current with the bottom stress, whereas on ebb tide, the along-channel stress is positive (~5 cm^2 s^{-2}), representing a reverse transport of horizontal momentum. Vertically, in general the along-channel stress decreases with distance from the seafloor, but there were occasions when large stress occurred above the mid-depth. These events were results of complex structure of the velocity shear (Figure 3(c) and (d)), possibly associated with the estuarine circulation and wind-driven currents.

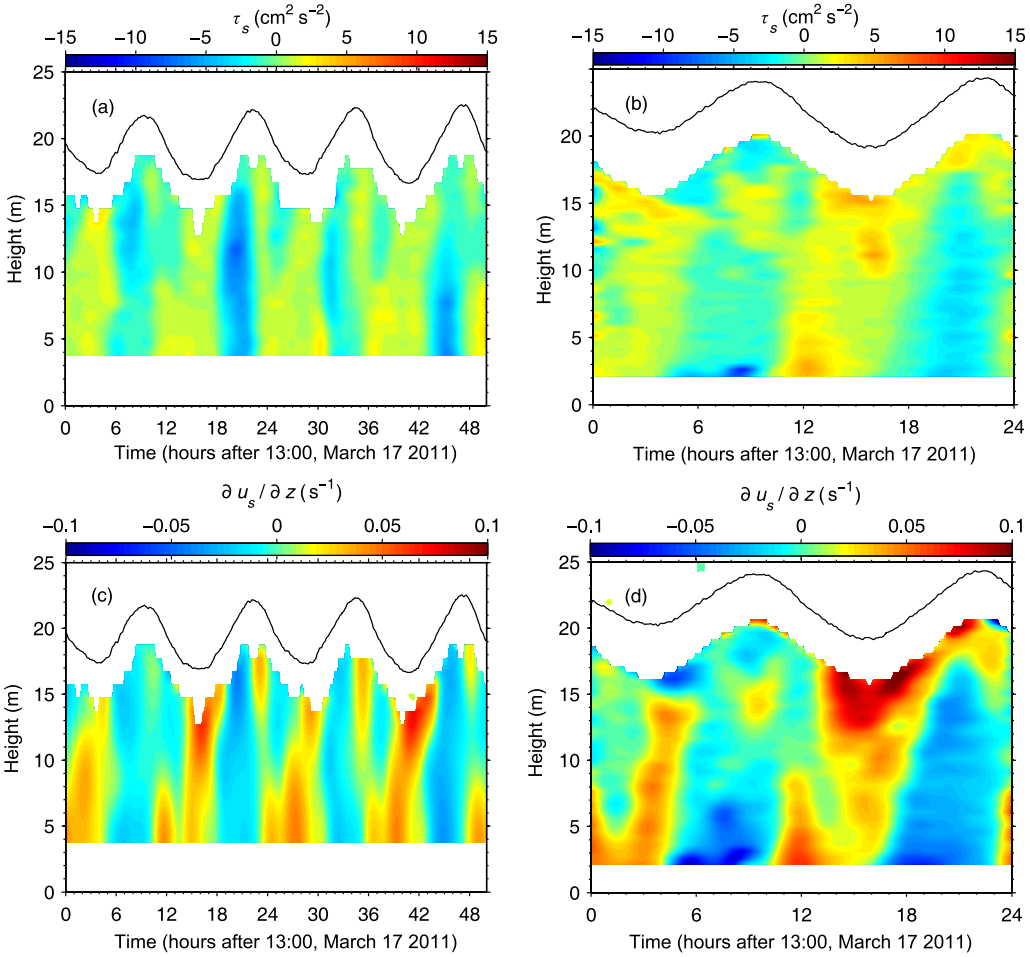

Figure 3 Along-channel Reynolds stress τ_s and corresponding vertical shear of the mean flow $\partial u_s/\partial z$ at Sts. A1 and A2. (a), (b) Along-channel Reynolds stress; (c), (d) vertical shear of the mean flow.

3.2 Production and dissipation rates of the TKE

The interaction of Reynolds stress with the shear of mean flow leads to a shear production of TKE, i.e., the shear production P, which is roughly in balance with the viscous dissipation rate of the TKE for unstratified shear flows, i.e., $P \approx \varepsilon$. The production and dissipation rates of the TKE at the three stations are shown in Figure 4.

Figure 4(a) and (b) shows the production rate (P) at Sts. A1 and A2. It is evident that there was a pronounced M_4 cycle in P, with evident ebb-flood asymmetry. During the flood, large values of P (~5×10^{-6} W kg^{-1}) were observed all through the water column, suggesting a high transfer rate of kinetic energy from the mean flow to turbulent fluctuations. In contrast, during the ebb, large production rate (~1×10^{-6} W kg^{-1}) was confined only to a 5–8 m thick bottom boundary layer, in which P generally decreases with distance from the seafloor. Another aspect of the ebb-flood asymmetry in P is evident in its features at successive slack waters. Around high slack water, the production rates were small (~3×10^{-8} W kg^{-1}), suggesting weak shear of the mean flow and negligible Reynolds stress. However, around low slack water, large production rate (Figure 4(b)) occurred at 2–5 m below the surface, corresponding to high Reynolds stress and velocity shear.

Figure 4(c) and (d) shows the observed (ε_{MSS}) and simulated (ε_{SMC}) TKE dissipation rate at St. M3. The simulation was based on the k-ε model with stability function proposed by Canuto et al. (2001). The model was forced by realistic flow and stratification from the observations. For simplicity, constant horizontal density gradients were used to reproduce the observed variations of stratification.

As shown in Figure 4(c) and (d), the M_4 cycle in the TKE dissipation rate ε was also very evident, with the bottom boundary layer being characterised by high ε (~5×10^{-6} W kg^{-1}). Around high slack water, however, ε in the whole water column was much weaker (~5×10^{-8} W kg^{-1}), as tidal current was very weak. A comparison of ε_{MSS} and ε_{SMC} suggests that the turbulent closure model tends to overestimate ε in the bottom boundary layer. This is due mainly to the inaccurate parameterization of upward TKE transport from the near-bed region. Moreover, the effect of wind stress, buoyancy flux, surface wave breaking, and Langmuir circulation on near-surface turbulence has been neglected in the model, which may have significant contributions to the

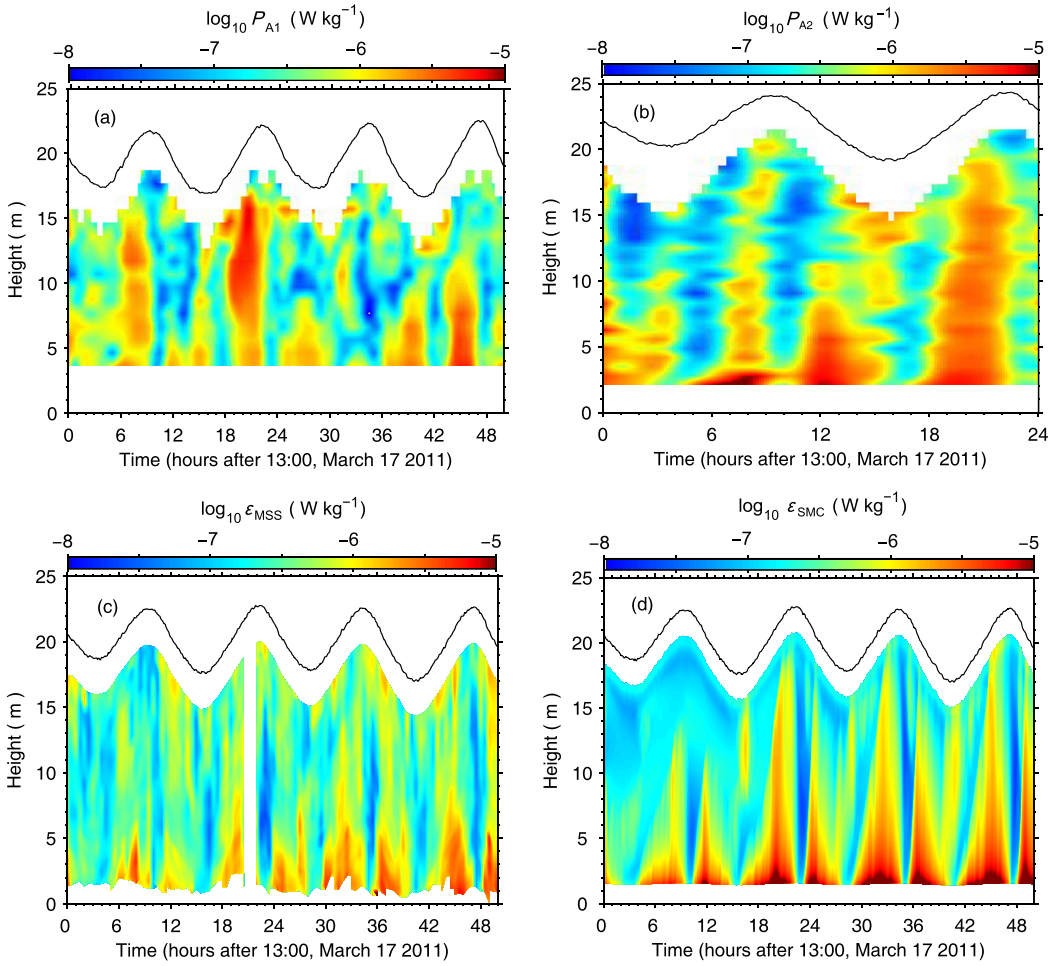

Figure 4 Contour plots of the rate of production ((a), (b)) and dissipation ((c), (d)) of TKE. Note that the blank band in (c) was due to a lack of data.

observed turbulent dissipation.

3.3 Vertical eddy viscosity

The eddy viscosity at Sts. A1 (υ_t^{A1}), A2 (υ_t^{A2}) and M3 (υ_t^{SMC} and υ_t^{SMC}) is shown in Figure 5. It can be seen that they generally agree with each other, all subject to very similar temporal variations to the Reynolds stress (Figure 3(a) and (b)). During the flood, large values of υ_t were found all through the water column, with a magnitude of about 10^{-2} m^2 s^{-1}; whereas during the ebb, large values of υ_t were only located within a 5–8 m thick bottom boundary layer. This ebb-flood asymmetry of turbulence, however, was not evident in Figure 5 (c). This suggests that some of the assumptions adopted in the calculations may be invalid. For example, the mixing efficiency Γ may be subject to dramatic changes, rather than keeping a constant value of 0.2 as we assumed, within the tidal cycle, and there may be significant temporal variations or transport of the TKE that formally broke the assumed local balance of TKE. An important indication is, even though we can obtain reliable estimates of the TKE dissipation rates from turbulence profiling measurements, knowledge on mixing efficiency Γ is required to have reliable estimates of the turbulent fluxes of momentum, buoyancy and materials. This has been in fact a bottleneck of ocean turbulence studies, and should be explored in further studies.

4 Discussion

As shown above, there was evident ebb-flood asymmetry in all the analysed turbulence quantities. This is in fact frequently observed in freshwater-influenced coastal embayments; for example, the Liverpool Bay (Rippeth et al., 2001), the San Francisco Bay (Stacey et al., 1999a), and the Hudson River (Nepf and Geyer, 1996). To gain a qualitative understanding on the dynamic mechanism of this asymmetry, we consider temporal variations of stratification in terms of the potential energy anomaly ϕ (Simpson et al., 1990)

$$\phi = \frac{1}{H}\int_{-h}^{\eta} gz\left(\overline{\rho} - \rho(z)\right)\mathrm{d}z = -\frac{1}{H}\int_{-h}^{\eta} gz\tilde{\rho}(z)\mathrm{d}z, \quad (12)$$

$$\overline{\rho} = \frac{1}{H}\int_{-h}^{\eta} \rho_{(z)}\mathrm{d}z, \quad (13)$$

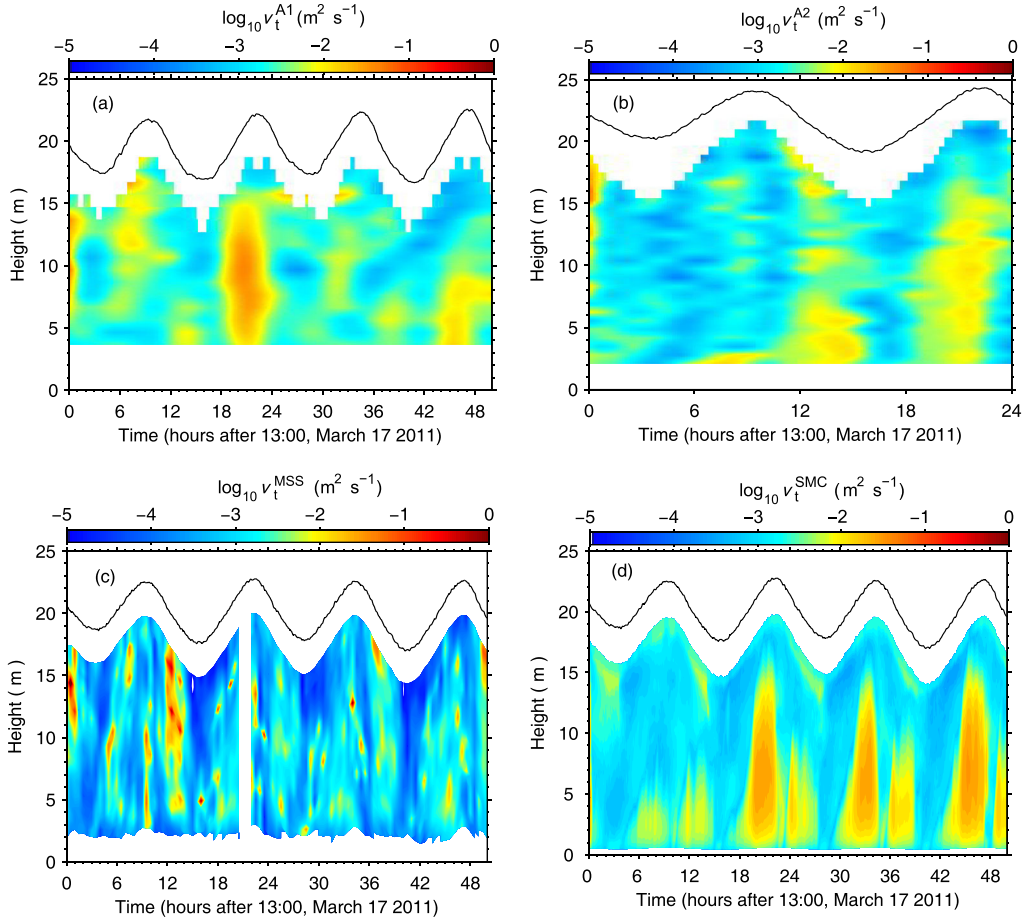

Figure 5 Vertical eddy viscosity at Sts. A1, A2 and M3. (a) vertical eddy viscosity at St. A1 based on eq. (4); (b) vertical eddy viscosity at St. A2 based on eq. (4); (c) vertical eddy viscosity at St. M3 based on eq. (7); (d) vertical eddy viscosity at St. M3 simulated with SMC model.

where ϕ (units: J m^{-3}) represents the amount of work required to bring about complete vertical mixing per unit volume. It increases positively with water column stratification. $\overline{\rho}$ is the depth-averaged density; $\tilde{\rho}(z)$ is the deviation from the depth mean value over the water column of depth H, given by $H=h+\eta$, η the free surface, and h the mean water depth.

From the transport equations of the potential temperature, salinity and the continuity equation, the transport equation of ϕ can be obtained (de Boer et al., 2008)

$$\frac{\partial \phi}{\partial t} = \underbrace{\frac{g}{H}\frac{\partial \overline{\rho}}{\partial s}\int_{-h}^{\eta}\left(u_s(z)-\overline{u}_s\right)z\mathrm{d}z}_{S_s} + \underbrace{\frac{g}{H}\frac{\partial \overline{\rho}}{\partial n}\int_{-h}^{\eta}\left(u_n(z)-\overline{u}_n\right)z\mathrm{d}z}_{S_n} + \underbrace{\frac{\rho_0}{H}\int_{-h}^{\eta}\left(\frac{g}{\rho_0}\upsilon_t'\partial_z\rho\right)\mathrm{d}z}_{M_z} + \underbrace{\cdots}_{\mathrm{RES}}, \quad (14)$$

where, S_s and S_n are the along-shore and cross-shore straining terms. They describe the deformation of vertically uniform horizontal density gradient by velocity shear. The term M_z describes the effect of vertical mixing on the density profile. RES is used to denote all remaining terms contributing to temporal variations of ϕ such as the advection of horizontal density gradients, non-linear shear dispersion terms and a term related to upwelling and downwelling. For precise definition of all of these terms, readers are referred to de Boer et al. (2008).

To illustrate the asymmetric feature of turbulent mixing in the Xiamen Bay, we calculate the depth average of the vertical eddy viscosity at St. A1. Figure 6 (a) shows the resulting time series of $\overline{\upsilon}_t$, which clearly shows ebb-flood asymmetry over four tidal cycles. Within one tidal cycle, turbulent mixing is stronger during flood than during ebb tides.

The time series of the potential energy anomaly ϕ is shown in Figure 6(b). As expected, ϕ showed a clear tidal cycling. It decreased during flood tide whereas increased during ebb tide. With the onset of the ebb current, ϕ increased as a result of the differential advection of water-mass; lighter surface water moved faster seaward and overtook heavier more saline water in the lower layer, thus gradually increasing stratification. On the flood, the process was reversed and the stratification induced on the ebb was gradually eliminated. As shown in Figure 6(b), ϕ was up to 34 J m^{-3} at the end of ebb, whereas it was less than 3 J m^{-3} by the end of flood.

Figure 6(d) shows the time series of different terms in the transport equation of the potential energy anomaly ϕ at St. A1. It can be seen that the variation of ϕ was controlled mainly by along-shore tidal straining, with the cross-shore straining and vertical mixing playing secondary roles. Tidal straining enhances stratification on the ebb but reduces stratification on the flood. Vertical mixing tends to reduce stratification all the time, but it is negligible as compared to tidal straining within a tidal cycle. However, at a longer time scale, the impact of vertical mixing is dominant in controlling the variation of water column stratification, and thus ϕ.

Here, the contribution of tidal straining was estimated with constant horizontal density gradients: $\partial\overline{\rho}/\partial s \approx 8.2\times10^{-5}$ kg m^{-4} and $\partial\overline{\rho}/\partial n \approx 3.0\times10^{-5}$ kg m^{-4}. Based on these gradients, the depth-averaged density simulated by the SMC model agrees quite well with the measurements (Figure 6(c)). The contribution of vertical mixing term M_z was determined by using a formulation related to the mixing efficiency Γ and TKE dissipation rate ε, see eq. (7).

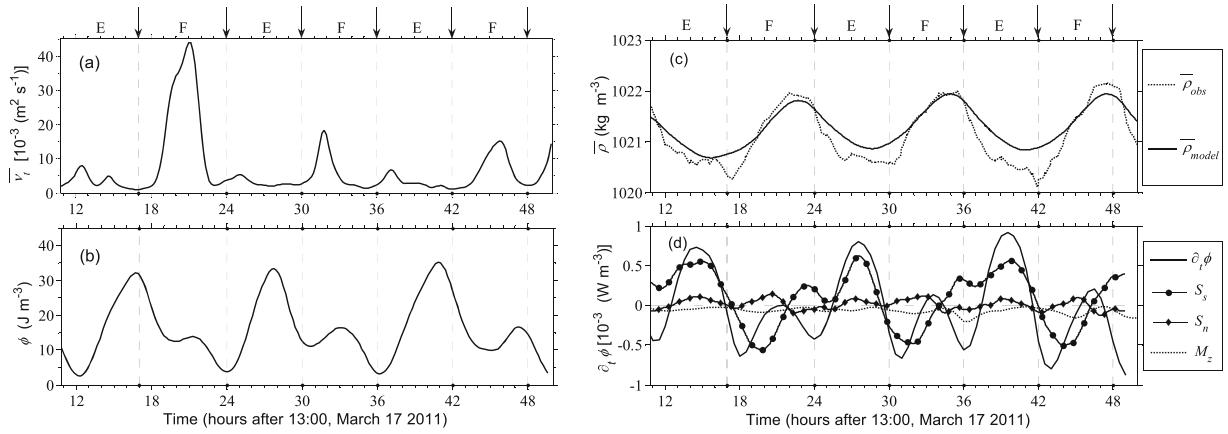

Figure 6 Temporal variation of the depth-averaged vertical eddy viscosity $\overline{\upsilon}_t$ at St. A1 (a); time series of the potential energy anomaly ϕ (b); observed and simulated results of the depth-mean density with a horizental density gradient (c): $\partial\overline{\rho}/\partial s \approx 8.2\times10^{-5}$ kg m^{-4} and $\partial\overline{\rho}/\partial n \approx 3.0\times10^{-5}$ kg m^{-4}; evolution of the individual terms in eq. (14) (d). The vertical dot-lines show the transition between flood and ebb tides.

To assess the capability of second-moment turbulence closure models in modeling turbulence processes in this weakly stratified tidally energetic environment, we compare the depth-averaged TKE dissipation rate simulated with the SMC model with observation-based estimates from the MSS and ADCP data. They are shown in Figure 7. The time series of water depth is shown in Figure 7(a), to provide a reference to tidal phase for other time series plots. Figure 7(b) shows the time series of observed and simulated stratification, expressed as the density difference $\Delta\rho$ between 15 and 5 m above the seafloor. A constant horizontal density gradient was adopted to reproduce observed tidal variations of stratification with a 1D water column model. As clearly shown in Figure 7(b), the model successfully captured main features of stratification variation. Figure 7(c) shows the time series of the depth-averaged production (P) and dissipation (ε) rates of TKE over two tidal cycles. Overall, the consistency between the modeled and different estimates of turbulence quantities is pretty good, suggesting that the SMC model can capture main features of turbulence in this dynamic regime. However, discrepancies among them are also evident. This is due partly to the approximations and assumptions adopted in both the numerical simulation and observation-based estimates, but also reflects the problems inherent in the SMC model. Further refinements of the SMC model are obviously needed, but observational estimates of turbulence quantities based on more-relaxed theoretical assumptions are also very important to make the observation and numerical simulation directly comparable.

5 Conclusions

In this study, turbulence and mixing in the Xiamen Bay, a freshwater-influenced tidal bay located at the west side of the Taiwan Strait, were investigated with both *in situ* measurements and numerical simulations. The former includes 50-h continuous turbulence profiling measurements at one station (M3), and both velocity and turbulence measurements with bottom-mounted ADCP at two other nearby stations (A1 and A2). As such, time series of the Reynolds stress, production and dissipation rates of the turbulent kinetic energy, as well as the vertical eddy viscosity, through the whole water column, were obtained. This allows us on one hand for the first time to have an understanding of turbulence and mixing characteristics in the Xiamen Bay based on direct measurements, and on the other hand to test the capability of the state-of-the-art second-moment turbulence closure schemes in simulating turbulence and mixing in tidally energetic weakly stratified coastal environment.

The flows in the Xiamen Bay were driven mainly by the semi-diurnal M_2 tide, which generates rectilinear tidal currents with a speed up to 0.9 m s^{-1}. As a result, all the turbulence quantities were subject to significant tidal (M_4) variations, but with evident ebb-flood asymmetry. For example, during the flood, the magnitude of the along-channel Reynolds stress was up to 10 cm^2 s^{-2}, whereas during the ebb, it was only 5 cm^2 s^{-2}. Diagnosis of the potential energy anomaly showed that the asymmetrical tidal mixing was induced mainly by tidal straining, which reduces stratification during the flood and enhances stratification during the ebb, thus modulating turbulence and mixing processes in the water column.

Forced by realistic currents and stratification from the measurements, a k-ε model was used to simulate turbulence and mixing within the observational period. The model can successfully reproduce both tidal variations and asymmetric features of the turbulence quantities, providing direct

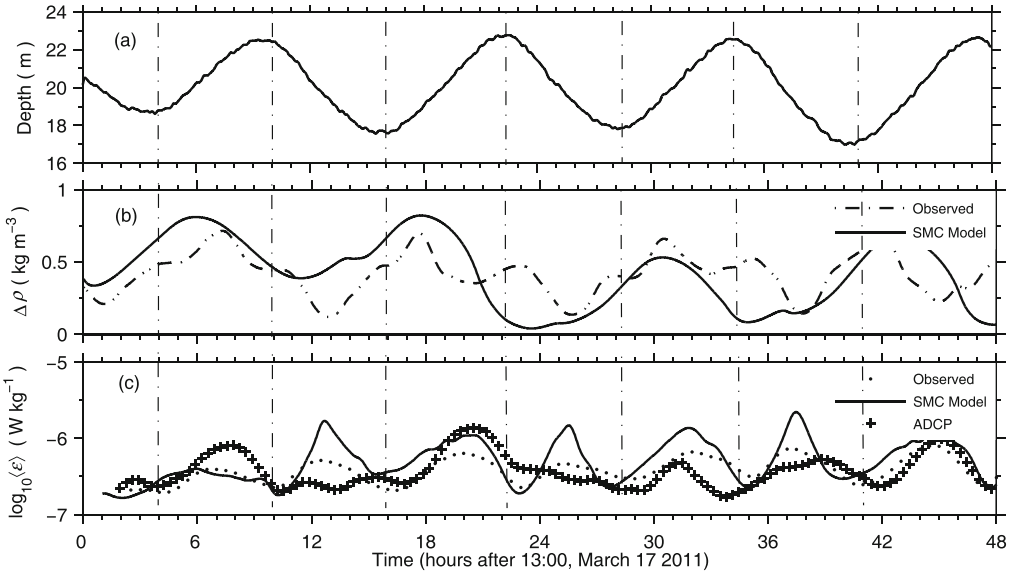

Figure 7 Time series of the water depth at St. M3 (a); observed and simulated stratification expressed as the density difference between 15 and 5 m above the seafloor (b); the depth-averaged production and dissipation rate estimated from the microstructure profiliing data, ADCP data and the SMC model (c).

support for the usefulness of turbulence closure schemes. There are, however, obvious discrepancies between the observations and model results. Further refinements of the turbulence closure schemes are obviously needed to fully capture the complex dynamic processes in the freshwater-influenced tidally driven coastal embayments.

This work was supported by the National Natural Science Foundation of China (Grant Nos. 41006017, 41476006), and the Natural Science Foundation of Fujian Province of China (Grant No. 2015J06010). We thank the crew of the RV Haiyang-2, Wang Jianing, and Sun Zhenyu for their assistance in data collection. Turbulence simulations were conducted with the General Ocean Turbulence Model (GOTM).

Burchard H, Bolding K. 2001. Comparative analysis of four second-moment turbulence closure models for the oceanic mixed layer. J Phys Oceanogr, 31: 1943–1968

Canuto V M, Howard A, Cheng Y, et al. 2001. Ocean turbulence. Part I: One-point closure model-momentum and heat vertical diffusivities with and without rotation. J Phys Oceanogr, 31: 1413–1426

de Boer G J, Pietrzak J D, Winterwerp J C. 2008. Using the potential energy anomaly equation to investigate the roles of tidal straining and advection in river plumes. Ocean Model, 22: 1–11

Dewey R K, Crawford W R, Gargett A E, et al. 1987. A microstructure instrument for profiling oceanic turbulence in coastal bottom boundary layers. J Atmos Ocean Tech, 4: 288–297

Fisher N R, Simpson J H, Howarth M J. 2002. Turbulent dissipation in the Rhine ROFI forced by tidal flow and wind stress. J Sea Res, 48: 249–258

Kraus E B, Turner J S. 1967. A one-dimensional model of the seasonal thermocline. Tellus, 19: 98–106

Liu Z Y, Wei H, Lozovatsky I D, et al. 2009. Late summer stratification, internal waves, and turbulence in the Yellow Sea. J Mar Syst, 77: 459–472

Lohrmann A, Hackett B, Roed L P. 1990. High-resolution measurements of turbulence, velocity, and stress using a pulse-to-pulse coherent sonar. J Atmos Ocean Tech, 7: 19–37

Lu Y, Lueck R G. 1999a. Using a broadband ADCP in a tidal channel. Part I: Mean flow and shear. J Atmos Ocean Tech, 16: 1556–1567

Lu Y, Lueck R G. 1999b. Using a broadband ADCP in a tidal channel. Part II: Turbulence. J Atmos Ocean Tech, 16: 1568–1579

Lucas N S, Simpson J H, Rippeth T P, et al. 2014. Measuring turbulent dissipation using a tethered ADCP. J Atmos Ocean Tech, 31: 1826–1837

Lueck R G, Wolk F, Yamazaki H. 2002. Oceanic velocity microstructure measurements in the 20th century. J Oceanogr, 58: 153–174

Nepf H M, Geyer W R. 1996. Intratidal variations in stratification and mixing in the Hudson estuary. J Geophys Res, 101: 12079–12086

Prandke H, Stips A. 1998. Test measurements with an operational microstructure-turbulence profiler: Detection limits of dissipation rates. Aquat Sci, 60: 191–209

Pope S B. 2000. Turbulent Flows. Cambridge: Cambridge University Press

Rippeth T P, Fisher N, Simpson J H. 2001. The cycle of turbulent dissipation in the presence of tidal straining. J Phys Oceanogr, 31: 2458–2471

Rippeth T P, Simpson J H, Williams E. 2003. Measurement of the rates of production and dissipation of turbulent kinetic energy in an energetic tidal flow: Red Wharf Bay revisited. J Phys Oceanogr, 33: 1889–1901

Schmitt F G. 2007. About Boussinesq's turbulent viscosity hypothesis: Historical remarks and a direct evaluation of its validity. CR Mecaniq, 335: 617–627

Simpson J H, Brown J, Matthews J, et al. 1990. Tidal straining, density currents, and stirring in the control of estuarine stratification. Estuaries, 13: 125–132

Simpson J H, Burchard H, Fisher N R, et al. 2002. The semi-diurnal cycle of dissipation in a ROFI: Model-measurement comparisons. Cont Shelf Res, 22: 1615–1628

Simpson J H, Crawford W R, Rippeth T P, et al. 1996. The vertical structure of turbulent dissipation in shelf seas. J Phys Oceanogr, 26: 1580–1590

Simpson J H, Green J A M, Rippeth T P, et al. 2009. The structure of dissipation in the western Irish Sea front. J Marine Syst, 77: 428–440

Simpson J H, Sharples J, Rippeth T P. 1991. A prescriptive model of stratification induced by freshwater run-off. Estuar Coast Shelf Sci, 33: 23–35

Stacey M T, Monismith S G, Burau J R. 1999a. Observations of turbulence in a partially stratified estuary. J Phys Oceanogr, 29: 1950–1970

Stacey M T, Monismith S G, Burau J R. 1999b. Measurements of Reynolds stress profiles in unstratified tidal flow. J Geophys Res, 104: 10933–10949

Thorpe S A. 2007. An Introduction to Ocean Turbulence. Cambridge: Cambridge University Press

Umlauf L, Burchard H. 2005. Second-order turbulence closure models for geophysical boundary layers: A review of recent work. Cont Shelf Res, 25: 795–827

Wilcox D C. 1998. Turbulence Modeling for CFD. 2nd ed. La Canada, CA: DCW Industries